HHS Public Access

Author manuscript

*Curr Biol*. Author manuscript; available in PMC 2018 March 06.

Published in final edited form as:

*Curr Biol*. 2017 March 06; 27(5): 688–696. doi:10.1016/j.cub.2017.01.013.

# Coordination of Orofacial Motor Actions into Exploratory Behavior by Rat

**Anastasia Kurnikova**[1,7], **Jeffrey D. Moore**[2,3,7], **Song-Mao Liao**[2], **Martin Deschênes**[4], and **David Kleinfeld**[2,5,6,8,*]

[1]Neurosciences Graduate Program, University of California San Diego, La Jolla, CA 92093, USA

[2]Department of Physics, University of California, San Diego, La Jolla, CA 92093, USA

[3]Department of Molecular and Cellular Biology, Harvard University, Cambridge, MA 02138, USA

[4]Centre de Recherche Université Laval Robert-Giffard, Québec City, Québec G1J 2R3, Canada

[5]Section of Neurobiology, University of California, San Diego, La Jolla, CA 92093, USA

[6]Department of Electrical and Computer Engineering, University of California, San Diego, La Jolla, CA 92093, USA

## SUMMARY

The delineation of sensorimotor circuits that guide exploration begins with an understanding of the pattern of motor outputs [1]. These motor patterns provide a clue to the form of the underlying circuits [2–4] (but see [5]). We focus on the behaviors that rodents use to explore their peripersonal space through goal-directed positioning of their nose, head, and vibrissae. Rodents sniff in response to novel odors, reward expectation, and as part of social interactions [6–12]. Sniffing serves olfaction [13, 14], while whisking synchronized to sniffing serves vibrissa-based touch [6, 15, 16]. We quantify the ethology of exploratory nose and head movements in relation to breathing. We find that sniffing is accompanied by prominent lateral and vertical de-flections of the nose, i.e., twitches, which are driven by activation of the *deflector nasi* muscles [17]. On the timescale of individual breaths, nose motion is rhythmic and has a maximum deflection following the onset of inspiration. On a longer timescale, excursions of the nose persist for several breaths and are accompanied by an asymmetry in vibrissa positioning toward the same side of the face. Such directed deflections can be triggered by a lateralized source of odor. Lastly, bobbing of the head as the animal cranes and explores is phase-locked to sniffing and to movement of the nose.

*Correspondence: dk@physics.ucsd.edu.
[7]Co-first author
[8]Lead contact

**EXPERIMENTAL PROCEDURES**

We report data from Long Evans adult female rats. Details of our methodology are in Supplemental Experimental Procedures.

SUPPLEMENTAL INFORMATION

Supplemental Information includes four figures and Supplemental Experimental Procedures and can be found with this article online at http://dx.doi.org/10.1016/j.cub.2017.01.013.

**AUTHOR CONTRIBUTIONS**

All authors planned the experiments. A.K., S.-M.L., and J.D.M. carried out the measurements and associated data analysis. D.K., A.K., and J.D.M. drafted the manuscript. D.K. attended to the myriad of university rules and forms that govern environmental health and safety issues as well as the ethical use of animals.

These data, along with prior results on the resetting of the whisk cycle at the onset of inspiration [15, 16, 18], reveal that the onset of each breath initiates a “snapshot” of the orofacial sensory environment.

## In Brief

Kurnikova et al. examine orofacial movement in rats during exploration. They find that deflections of the nose, head, and vibrissa have a fast component of motion that is locked to the breathing cycle, along with a slower, orienting component. These data indicate that each breath initiates a “snapshot” of the orofacial sensory environment.


## RESULTS

Rats sniff as they explore, where sniffing is taken as breathing rates greater than 4 Hz. In contrast, basal respiration is relatively slow, conservatively taken as rates of less than 2 Hz. We measure the position of the nose versus time, concurrent with measurements of breathing, in head-restrained animals (Figure 1A). As the rat sniffs, we observe two components of nose movement in the lateral and vertical directions. One is a slowly varying “bias” in nose positioning and the other a smaller rhythmic nose movement that is centered around the slowly varying bias in mean position (Figure 1B). We correlate the rhythmic component of nose motion to breathing where we separate bouts of sniffing from basal breathing. We find that the time to reach to maximum excursion, for both lateral and vertical nose positions, occurs slightly after the onset of inspiration (n = 3 rats) (Figure 1C). The maximum speed of the movement in the lateral directions occurs during expiration for sniffing and just prior to inspiration during basal respiration (Figure 1C). Consistent with this, the coherence of lateral and vertical nose speed to breathing is statistically significant at the sniffing frequencies and has a phase shift close to π radians (Figures S1E and S1F). Lastly, we note that motion of the nose in the third, rostrocaudal direction is found to

correlate with vertical motion and thus not considered for future analysis (Figure S1D). These findings establish the basic coordination of nose movement with sniffing.

Further insight into the rhythmic motion of the nose is found from a scatterplot of the maximum excursions of the nose in the lateral direction relative to the onset of breathing. The times corresponding to the maximal excursion were plotted in relation to the onset of inspiration, with trials sorted by breathing rate (n = 3 rats) (Figure 1D). We observe that the peak excursion occurs at a fixed time after the initial and second inspiration, as seen in the correlation (Figure 1C). In an interval where breathing is slower, i.e., 2 to 4 Hz (gray band in Figure 1D), we see that the position of the nose obtains an additional peak excursion at a fixed interval after the first breath but before the next breath (★ in Figure 1D). The presence of this additional peak is highly suggestive of an underlying oscillator for rhythmic nose movement that can function independently of the breathing rhythm. Analogous to the case for whisking [15], this hypothetical oscillator is reset by breathing.

We now turn to the slowly varying bias in lateral and vertical displacements of the nose that accompany sniffing but rarely occur during basal respiration (Figure 1E). Lateral nose displacements occur in both directions in the range of approximately ± 2 mm, while vertical displacements occur in the range of 0 to 2 mm (Figure 1E). The typical duration of bias in the direction of lateral nose motion is found by averaging right-and left-initiated movements that are aligned to the onset of each sniffing bout; onsets are identified as an abrupt increase in breathing rate by at least 1.5 Hz (Figure 1F). We find that both right and left excursions of the nose have a persistence time of 0.7 s, or about three sniff cycles, for ~0.7 of the movements and a persistence time of ~7 s for ~0.3 of the movements (n = 6 rats) (Figure S1G). Over 0.6 to 0.7 s, the nose tends to move 0.5 to 0.6 mm with a characteristic average speed of 0.9 mm/s (Figures 1F and S1H and S1I), although the characteristic maximum speed is much greater, i.e., 3 mm/s (Figures S1H and S1J).

A point of interest is that the relation between the displacement and instantaneous speed of the nose is well described by a power law (Figure 1G). This takes the form

$$\text{speed} \propto (\text{displacement})^{0.63 \pm 0.03}.$$

The exponent is close to 2/3, suggestive of motion control that minimizes jerk, the derivative of acceleration, along the movement trajectory of the nose [19].

What is the nature of the motor plant that drives motion of the nose? Past work showed that artificial activation of the *deflector nasi* (*d. nasi*) muscles elicits lateral and vertical movement of the nose [17]. To understand the role of these muscles as the rat explores, we performed simultaneous recordings of the electromyogram (EMG) of *d. nasi* on both sides of the face concurrent with videography of the head-restrained rat (Figure 2A). Typically both muscles are active. In the extreme, unilateral EMG activity of *d. nasi* leads to a combined ipsilateral and vertical deflection (★ in Figure 2B), while bilateral activity pulls the nose upward (+ in Figure 2B). More generally, our results suggest a model in which each *d. nasi* deflects the nose ipsilaterally and upward and the resulting nose position is a vector

sum of the activation of the *d. nasi* on each side (Figure 2C). Additional details of the muscular control are revealed by a correlation analysis across data from all animals (n = 3) (Figure 2D). First, we performed a cross correlation of the ipsi- and contralateral *d. nasi* EMG envelopes. We observe a single peak at equal time, which indicated that the two muscles tend to be co-activated. Second, the peak of the cross-correlation between the envelope of the *d. nasi* EMG to lateral nose motion occurred with a mean lag of 45 ± 5 ms (mean ± SEM) (insert in Figure 2D), with a similar result for the vertical motion. This value reflects the viscoelastic time-constant of the nasal cartilage.

The timing between nose motion and whisking was explicitly revealed by recording the EMG in the *d. nasi* muscles simultaneously with the EMG from two muscles in the vibrissa motor plant. The intrinsic muscles are predominantly responsible for protraction during sniffing [20], while the *nasolabialis* muscle retracts the mystacial pad and is one of two muscle groups that contributes to active retraction during sniffing [20, 21]. The EMGs were sorted according to ipsilateral versus contralateral deflection of the nose with respect to the side of recording, and we computed the average response of each muscle with respect to the onset of inspiration (Figure 2E). The envelope of the *d. nasi* EMG is observed to reach a peak value prior to the onset of inspiration (Figure 2E). The activation of the *d. nasi* muscle is stronger during ipsilateral versus contralateral movement such that the difference of the sorted signals reaches a peak ~55 ms prior to that of the nose position; this time difference is consistent with the directly measured delay between muscle activity and movement of 45 ± 5 ms (Figure 2E). Our measurement of the two sets of muscles that comprise the motor plant for whisking support past data. First, the envelope of the EMG for the intrinsic muscles tracks inspiration [15] and precedes the peak in protraction by ~23 ms [20]. Second, the envelope of the EMG for *nasolabialis* reaches a peak value prior to inspiration [16]. In new data, the peak displacement of the nose occurs ~40 ms prior to the maximum protraction of the vibrissa (Figure 2E). The bias in vibrissa and nose position occurs to the same side, i.e., during a sniff cycle the vibrissae ipsilateral to the nose deflection tend to be slightly retracted, by ~5° (Figure 2E). Lastly, activation of the *d. nasi* and the intrinsic muscles occurs essentially in anti-phase (Figure 2E).

Motion of the nose is likely to play a critical role in the localization of sources of odorants [6, 22, 23]. We thus quantified nose motion in response to the controlled delivery of fumes from bedding of the home cage (Figures S2A and S2B) alternately to the left or right nostril (Figures 3A and S2C). As a baseline response, we find that the rat begins to sniff and the nose lifts and deflects to the side of the presented odor (Figure 3B). The average response of the *d. nasi* muscles to an odor presented ipsilaterally or contralaterally shows that the ipsilateral muscle is strongly activated while the contralateral muscle is only weakly activated (Figures 3B and 3C). To confirm that the *d. nasi* muscles still activate in response to odor in the absence of head fixation, we repeated the measurement in body restrained rats. We found the same pattern of muscle activation, i.e., the ipsilateral muscle activated more strongly in response to lateralized odor presentation (Figures S2C and S2D). Finally, we consider the effect of blocking a nostril on the deflection of the nose. We first confirmed that blocking the nose on one side completely abolishes the breathing signal on that side (Figure 3D). Next, we recorded spontaneous nose motion. Consistent with curiosity-driven motor

actions, found that large deflections of the nose occurred primarily contralateral to the block and rarely to the blocked nostril (n = 5) (Figures 3E).

Beyond the slow change in the bias of the position of the nose (Figures 1F and 3C), slow changes in the amplitude and midpoint of whisking are well characterized [20, 21, 24]. We therefore consider the relationship between the lateral bias in nose position and the shift in the midpoint of whisking. We used head-restrained rats and tracked the angle of the C2 vibrissa on each side of the face (Figures 3F), along with measurements of nose position and breathing (Figure 1A). We find that the asymmetry in midpoint of the vibrissa motion between the two sides of the face is highly coherent with the bias in lateral movement of the nose (Figures 3G and S2E), such that right-to-left shifts in the midpoint slightly lead deflection of the nose (Figure S2F). We next used the odor presentation paradigm (Figure 3A) to determine whether the vibrissae respond to a laterally presented odor. We observe an increase in the amplitude of whisking concurrent with odor presentations and that, consistent with the deflection of the nose toward an odorant, the vibrissae bank in the direction of the odorant (Figure 3H). This is similar to the case observed for banking of the vibrissae as a rodent changes head direction [25, 26]. Finally, we note that relation of the asymmetry in whisking to nose motion is weak for the case of basal respiration (Figure S2F) as opposed to sniffing.

We extended our behavioral measurements to establish the composite relation among movements of the head, nose, and vibrissae, all with respect to the sniff cycle. We begin with unrestrained rats whose heads were outfitted with a gyrometer and EMG electrodes implanted bilaterally in the s*plenius capitis* muscles (Figure 4A), as well as a thermocouple as in the case of head-restrained rats (Figures 1A and 2A and 3A). The animals were placed on a small platform so that their body tended to remain still while they craned over the edges of the platform and performed successive head bobs (Figure 4A). Fumes from the home cage and other odors were presented to induce bouts of sniffing. We observe that the angular velocity of the head is dominated by rotations about the yaw and pitch axes, with only a small component of roll (Figures 4B and S3A). The cross-correlation between head speed and breathing demonstrates that head bobbing is coordinated with sniffing, with rhythmic movement of the head slowest at the midpoint of inspiration (Figure 4C). The peak head position occurs during inspiration and the full excursion of the rhythmic motion is estimated to be 0.4 mm (Figure S3B), close in value to the rhythmic excursion of the nose (Figure 1C). The cross-correlation between breathing and activation of the s*plenius capitis* activation demonstrates that head bobbing is driven by rhythmic contraction of neck muscles (Figures 4C and S3C and S3D), as opposed to motion of the torso secondary to breathing. At the level of motion along each axis, only yaw and pitch are phase-locked to breathing at the sniffing frequency while motion along all three axes is locked to basal breathing (Figure S3E). As with nose movement, we conjecture that the coordination of head movement with sniffing, with head speed at a minimum value during inspiration, minimizes the disruption of a potential plume of odorants during sampling.

The observation that both exploratory movements of the head (Figure 4C) and nose (Figure 1C) are coherent with breathing imply, but do not establish, that they are also coherent with each other. To independently verify that head and nose motion are in fact correlated, we

outfitted rats with an indwelling magnetic sensor of nose movement as well as a gyrometer (Figures 4D and S3F). The output of the probes change with shifts in magnetic field and thus reports nose position concurrent with measurements of head position (Figure 4E). We observe a significant peak in the spectral coherence between head and nose speed in the 6 to 9 Hz range of sniffing frequencies (Figure 4F), with a phase lag near $\pi/2$ radians, or a time lag of 30 ms at the peak frequency of 8 Hz. We conclude that nose movements are phase-locked to head movements during sniffing and that motion of the nose precedes that of the head.

The relative coordination among sniffing, nose motion, head bobbing, and whisking is summarized in a phase diagram (Figure 4G). The maximum vertical deflection of the nose and the maximum lateral deflection of the nose, to either side, occur during inspiration (Figure 1C), defined as the phase interval 0 to $\pi$ radians. The tilt of the head, found by integrating the angular velocity in the direction of pitch (Figure 4C), also reaches a peak during inspiration. Lastly, the protraction phase of whisking coincides with inspiration (Figure 3D). In toto, inspiration coordinates the orofacial motion that is used to sample a region of the peripersonal space that surrounds the rat's head.

## DISCUSSION

Our work establishes a scenario in which orofacial motor actions are choreographed relative to the sniff cycle, such that the onset of inspiration is coincident with a "snapshot" exploratory sampling (Figure 4G). In particular, we found rhythmic motion of the nose (Figures 1 and 2), i.e., twitching, as well as rhythmic motion of the head (Figure 4), i.e., bobbing, as the rodent cranes, are coordinated with sniffing through their respective muscular drive. The maximum upward deflection of the nose and head, as well as the protraction of the vibrissae, occur concurrent with inspiration (Figure 4G). Thus inspiration corresponds to a period of multisensory sampling of the environment. Head bobbing and nose twitching result in re-orientation of the head and nose during the expiratory phase of sniffing, so that the rodent can sample a new region of peripersonal space during the subsequent inspiratory phase. These data build on past findings on the coordination of whisking with sniffing [15, 16, 18] and expand beyond qualitative observations on bodily motion associated with sniffing [6]. Further, we show that a slow bias in the movement of the nose occurs during sniffing and that the nose orients toward odors (Figure 3). The *d. nasi* muscles contract synergistically to pull the nose laterally and upward and coordinate with breathing to cause the nose position to peak during inspiration (Figure 2).

Our results, together with past data on the resetting of the whisking rhythm by breathing [15, 16, 18], imply that respiratory circuits in the brainstem [27–29] act as a master oscillator to phase-lock rhythmic orofacial motor actions. What might be the utility of coordinating the fast, rhythmic motion of the different sensory apparatuses as animals explore their nearby environment? It is an open issue whether the coordination of these motor actions maximizes sensory input [30, 31], such as by sweeping odorants toward the nose. Any source of sensory input that contributes to both touch and olfaction, which are elements of social interactions [32] as well as exploration (Figure 4G), will lead to multisensory input that is likely to be phase-locked to breathing. The temporal regularity of the signals can improve the fidelity of

coding of the stimuli. The same argument holds for deflection of the vibrissae by wind and olfaction [33]. The issue of temporally synchronized signals issue might be potentially addressed by recordings from multisensory areas [31] using a rodent in a virtual environment [34].

The present work is focused on coordination of sensory input from proximal sources. How does this compare with coordination of input from distant sources, as detected by visual and acoustic disturbances? Saccadic eye movements and pinna movements, for example, are temporally coordinated with each other and serve to orient to a stimulus of either modality [35–37]. During coordinated eye-head movements in primates, the eye leads the head by 25 to 40 ms [36], similar to the latency between nose and head movements in rodents (Figure 4C). The need to reorient the head relative to the lighter and thus faster moving vibrissae, nose, and eyes thus appears to lead to similar phase-shifts for sensing of near as well as distant spatial scales.

What role might orientation of the nose play in olfactory perception? It has been shown that rats are able to quickly distinguish small differences in the lateral position of olfactory inputs [38] and are impaired on tracking and odor localization tasks when a nostril is blocked [13, 22]. This evidence suggests that even small air flow differences between nostrils, as might be generated by nose movement [39], could aid in odor tracking and source localization. While we have recently described the premotor circuitry for whisking and breathing [15, 16], the corresponding circuitry that supports the orientation and net deflection of other orofacial sensory organs during exploration remains to be delineated. For the present case of the nose, this circuitry presumably involves ascending input via the accessory olfactory nucleus [40].

## Supplementary Material

Refer to Web version on PubMed Central for supplementary material.

## Acknowledgments

We thank Beth Friedman and Harvey J. Karten for comments on an early version of the manuscript and Sebastian Haesler and Massimo Vergassola for discussions. This study was supported by grants from the Canadian Institutes of Health Research (MT-5877 to M.D.), the National Institute of Neurological Disorders and Stroke (NS058668 to D.K. and BRAIN NS0905905 to M.D. and D.K.), and the National Science Foundation (BRAIN EAGER 1451026 to D.K.). A.K. holds a Ruth L. Kirschstein National Research Service Award fellowship (NS089316) and J.D.M. is a fellow of the Jane Coffins Child Memorial Fund for Medical Research.

## References

1. Tinbergen, N. The Study of Instinct. New York: Oxford University Press; 1951.
2. Marder E, Calabrese RL. Principles of rhythmic motor pattern generation. Physiol Rev. 1996; 76:687–717. [PubMed: 8757786]
3. Kleinfeld, D., Sompolinsky, H. Associative network models for central pattern generators. In: Koch, C., Segev, I., editors. Methods in Neuronal Modeling: From Synapses to Networks. Cambridge: MIT Press; 1989. p. 195-246.
4. Doyle JC, Cseteb M. Architecture, constraints, and behavior. Proceeding of the National Academy of Sciences USA. 2011; 108(Sup 3)

5. Carandini M. From circuits to behavior: a bridge too far? Nat Neurosci. 2012; 15:507–509. [PubMed: 22449960]
6. Welker WI. Analysis of sniffing of the albino rat. Behaviour. 1964; 12:223–244.
7. Clarke S, Trowill JA. Sniffing and motivated behavior in the rat. Physiol Behav. 1971; 6:49–52. [PubMed: 4942174]
8. Brecht M, Freiwald WA. The many facets of facial interactions in mammals. Curr Opin Neurobiol. 2012; 22:259–266. [PubMed: 22209040]
9. Wachowiak M. All in a sniff: olfaction as a model for active sensing. Neuron. 2011; 71:962–973. [PubMed: 21943596]
10. Wolfe J, Mende C, Brecht M. Social facial touch in rats. Behav Neurosci. 2011; 125:900–910. [PubMed: 22122151]
11. Kepecs A, Uchida N, Mainen ZF. The sniff as a unit of olfactory processing. Chem Senses. 2006; 31:167–179. [PubMed: 16339265]
12. Prescott TJ, Diamond ME, Wing AM. Active touch sensing. Philosophical Transactions of the Royal Society of London B Biology (Basel). 2011; 366:2989–2995.
13. Khan AG, Sarangi M, Bhalla US. Rats track odour trails accurately using a multi-layered strategy with near-optimal sampling. Nat Commun. 2012; 3:703. [PubMed: 22426224]
14. Shusterman R, Smear MC, Koulakov AA, Rinberg D. Precise olfactory responses tile the sniff cycle. Nat Neurosci. 2011; 14:1039–1044. [PubMed: 21765422]
15. Moore JD, Deschênes M, Furuta T, Huber D, Smear MC, Demers M, Kleinfeld D. Hierarchy of orofacial rhythms revealed through whisking and breathing. Nature. 2013; 469:53–57.
16. Deschênes M, Takatoh J, Kurnikova A, Moore JD, Demers M, Elbaz M, Furuta T, Wang F, Kleinfeld D. Inhibition, not excitation, drives rhythmic whisking. Neuron. 2016; 90:374–387. [PubMed: 27041498]
17. Deschênes M, Haidarliu S, Demers M, Moore J, Kleinfeld D, Ahissar E. Muscles involved in naris dilation and nose motion in rat. Anat Rec (Hoboken). 2015; 298:546–553. [PubMed: 25257748]
18. Ranade S, Hangya B, Kepecs A. Multiple modes of phase locking between sniffing and whisking during active exploration. J Neurosci. 2013; 33:8250–8256. [PubMed: 23658164]
19. Wolpert DM. Computational approaches to motor control. Trends Cogn Sci. 1997; 1:209–216. [PubMed: 21223909]
20. Hill DN, Bermejo R, Zeigler HP, Kleinfeld D. Biomechanics of the vibrissa motor plant in rat: rhythmic whisking consists of triphasic neuromuscular activity. J Neurosci. 2008; 28:3438–3455. [PubMed: 18367610]
21. Berg RW, Kleinfeld D. Rhythmic whisking by rat: retraction as well as protraction of the vibrissae is under active muscular control. J Neurophysiol. 2003; 89:104–117. [PubMed: 12522163]
22. Catania KC. Stereo and serial sniffing guide navigation to an odour source in a mammal. Nat Commun. 2013; 4:1441. [PubMed: 23385586]
23. Deschênes M, Moore J, Kleinfeld D. Sniffing and whisking in rodents. Curr Opin Neurobiol. 2012; 22:243–250. [PubMed: 22177596]
24. Carvell GE, Simons DJ. Task- and subject-related differences in sensorimotor behavior during active touch. Somatosens Mot Res. 1995; 12:1–9. [PubMed: 7571939]
25. Towal RB, Hartmann MJ. Right-left asymmetries in the whisking behavior of rats anticipate head movements. J Neurosci. 2006; 26:8838–8846. [PubMed: 16928873]
26. Mitchinson B, Martin CJ, Grant RA, Prescott TJ. Feedback control in active sensing: rat exploratory whisking is modulated by environmental contact. Proc Biol Sci. 2007; 274:1035–1041. [PubMed: 17331893]
27. Smith JC, Abdala APL, Borgmann A, Rybak IA, Paton JFR. Brainstem respiratory networks: building blocks and microcircuits. Trends Neurosci. 2013; 36:152–162. [PubMed: 23254296]
28. Garcia AJ 3rd, Zanella S, Koch H, Doi A, Ramirez JM. Chapter 3–networks within networks: the neuronal control of breathing. Prog Brain Res. 2011; 188:31–50. [PubMed: 21333801]
29. Feldman JL, Del Negro CA. Looking for inspiration: new perspectives on respiratory rhythm. Nat Rev Neurosci. 2006; 7:232–242. [PubMed: 16495944]

30. Kleinfeld D, Moore JD, Wang F, Deschênes M. The brainstem oscillator for whisking and the case for breathing as the master clock for orofacial motor actions. Cold Spring Harb Symp Quant Biol. 2014; 79:29–39. [PubMed: 25876629]
31. Kleinfeld D, Deschênes M, Wang F, Moore JD. More than a rhythm of life: breathing as a binder of orofacial sensation. Nat Neurosci. 2014; 17:647–651. [PubMed: 24762718]
32. Lenschow C, Brecht M. Barrel cortex membrane potential dynamics in social touch. Neuron. 2015; 85:718–725. [PubMed: 25640075]
33. Yu YSW, Graff MM, Bresee CS, Man YB, Hartmann MJZ. Whiskers aid anemotaxis in rats. Sci Adv. 2016; 2:e1600716. [PubMed: 27574705]
34. Sofroniew NJ, Cohen JD, Lee AK, Svoboda K. Natural whisker-guided behavior by head-fixed mice in tactile virtual reality. J Neurosci. 2014; 34:9537–9550. [PubMed: 25031397]
35. Burr D, Alais D. Combining visual and auditory information. Prog Brain Res. 2006; 155:243–258. [PubMed: 17027392]
36. Bizzi E, Kalil RE, Tagliasco V. Eye-head coordination in monkeys: evidence for centrally patterned organization. Science. 1971; 173:452–454. [PubMed: 17770450]
37. Populin LC, Yin TCT. Pinna movements of the cat during sound localization. J Neurosci. 1998; 18:4233–4243. [PubMed: 9592101]
38. Rajan R, Clement JP, Bhalla US. Rats smell in stereo. Science. 2006; 311:666–670. [PubMed: 16456082]
39. Deschênes M, Kurnikova A, Elbaz M, Kleinfeld D. Circuits in the ventral medulla that phase lock motoneurons for coordinated sniffing and whisking. Neural Plasticity. 2016; 2016 ID 7493048.
40. Kikuta S, Sato K, Kashiwadani H, Tsunoda K, Yamasoba T, Mori K. From the Cover: Neurons in the anterior olfactory nucleus pars externa detect right or left localization of odor sources. Proc Natl Acad Sci USA. 2010; 107:12363–12368. [PubMed: 20616091]

## Highlights

- We quantify the ethology and muscular drive of exploratory nose and head movements
- Rhythmic twitching of the nose and bobbing of the head are phase locked to sniffing
- These onset of inspiration initiates a new sampling of peripersonal space
- Large excursions of the nose persist for several breaths and orient toward an odor

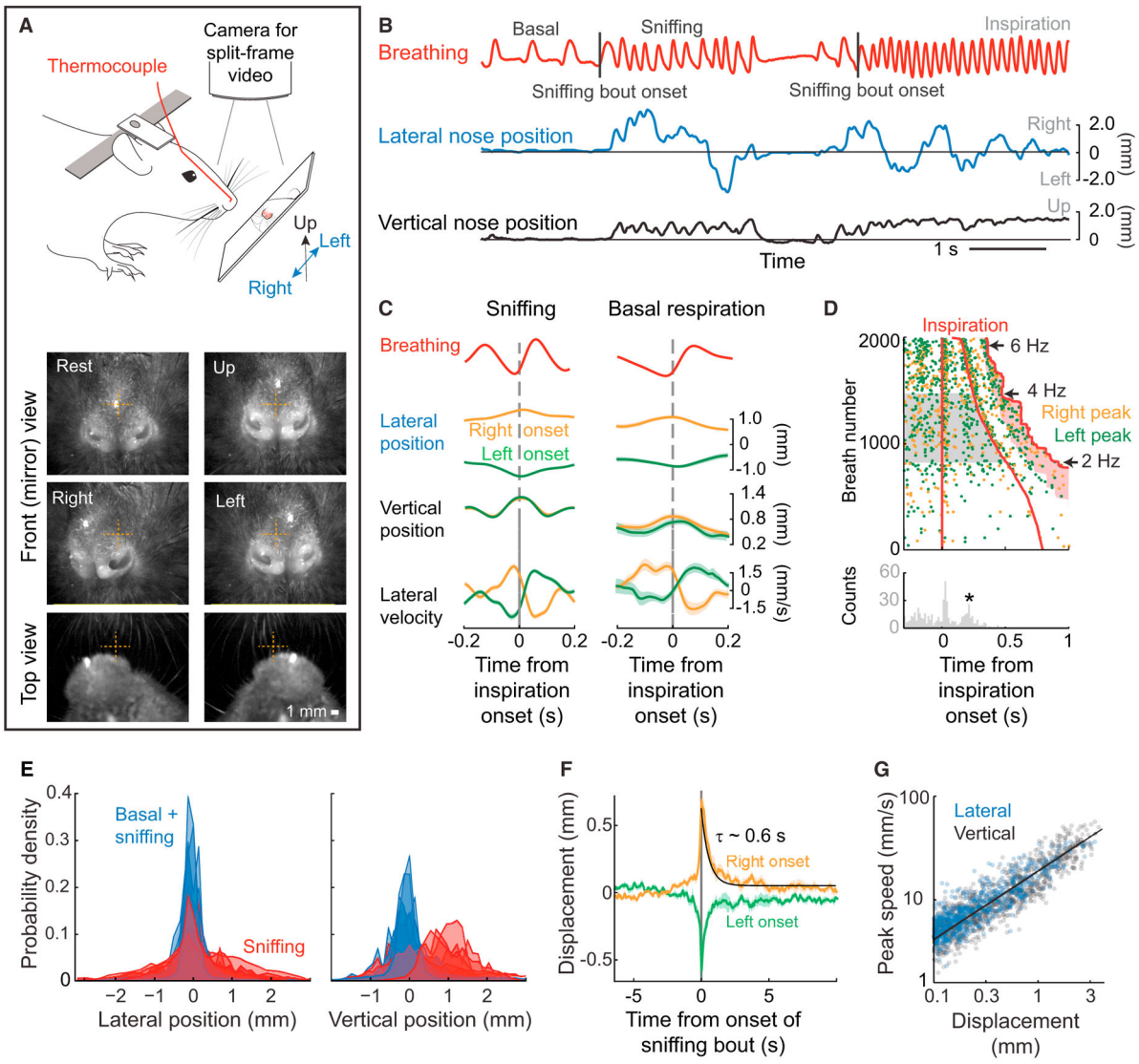


**Figure 1. Motion of the Nose**

(A) Schematic of the experimental setup for recording breathing and three-dimensional nose motion in a head restrained rat (top). A thermocouple is implanted in the nasal cavity to monitor breathing. A charge-coupled device (CCD) camera is mounted above rat, and a split frame is used to simultaneously image lateral and rostrocaudal nose motion from the top view, and lateral and vertical motion via a mirror in front of the rat that is set at 45 degrees (Figures S1A and S1B). Two example split frames and two additional front view frames are shown (bottom).

(B) A time series of breathing (red) along with lateral (blue) and vertical (black) nose motion. The nose tends to move during sniffing epochs and moves little during basal respiration. Sniffing bout onsets are marked by a tick.

(C) Inspiration triggered average of breathing (red) and nose motion (orange and green) for sniffing, i.e., 4 and 6 Hz breathing rate (left) and basal respiration, i.e., < 2 Hz breathing rate (right). Trials were selected for averaging as right-going (positive amplitude; orange) or left-

going (negative amplitude; green) if the value at the time of an inspiration onset was at least 0.5 mm from the center. Right- and left-going trials were averaged separately. Calculation performed with 560 trials (sniffing) and 98 trials (basal) of data across three rats; all error bars are SEM.

(D) Raster plot of nose lateral position peaks, thresholded with a 0.5 mm minimum displacement, in relation to the breath rise. Trials are sorted by breath duration and the direction of the lateral movement; right motion is orange and left motion is green. The histogram shows the time for the lateral motion to peak for intermediate breathing frequencies (2.0–4.0 Hz, highlighted in gray); only data prior to the second breath is included. The second peak in nose displacement (+) occurs 0.34 s after the onset of inspiration. Data are from a single animal.

(E) Histograms of the lateral and vertical nose positions for six rats. Blue histograms include values for both basal respiration and sniffing, while red histograms include only sniffing epochs.

(F) Average lateral position of the nose relative to the onset of a sniffing bout (B). Trials were sorted into right onset (orange) and left onset (green) by the average value within 100 ms of the sniffing bout onset. An exponential fit was calculated on the average of all traces, starting at time t = 0; black line.

(G) Scatterplot of the speed of lateral displacements versus the length of the displacement. Each length is defined by a starting and ending with a change in the sign of the velocity. Log-log plot; the line is a fit to the logarithm of the data with slope 0.63 ± 0.03, where the uncertainty is the 0.95 confidence interval.

See also Figure S1.

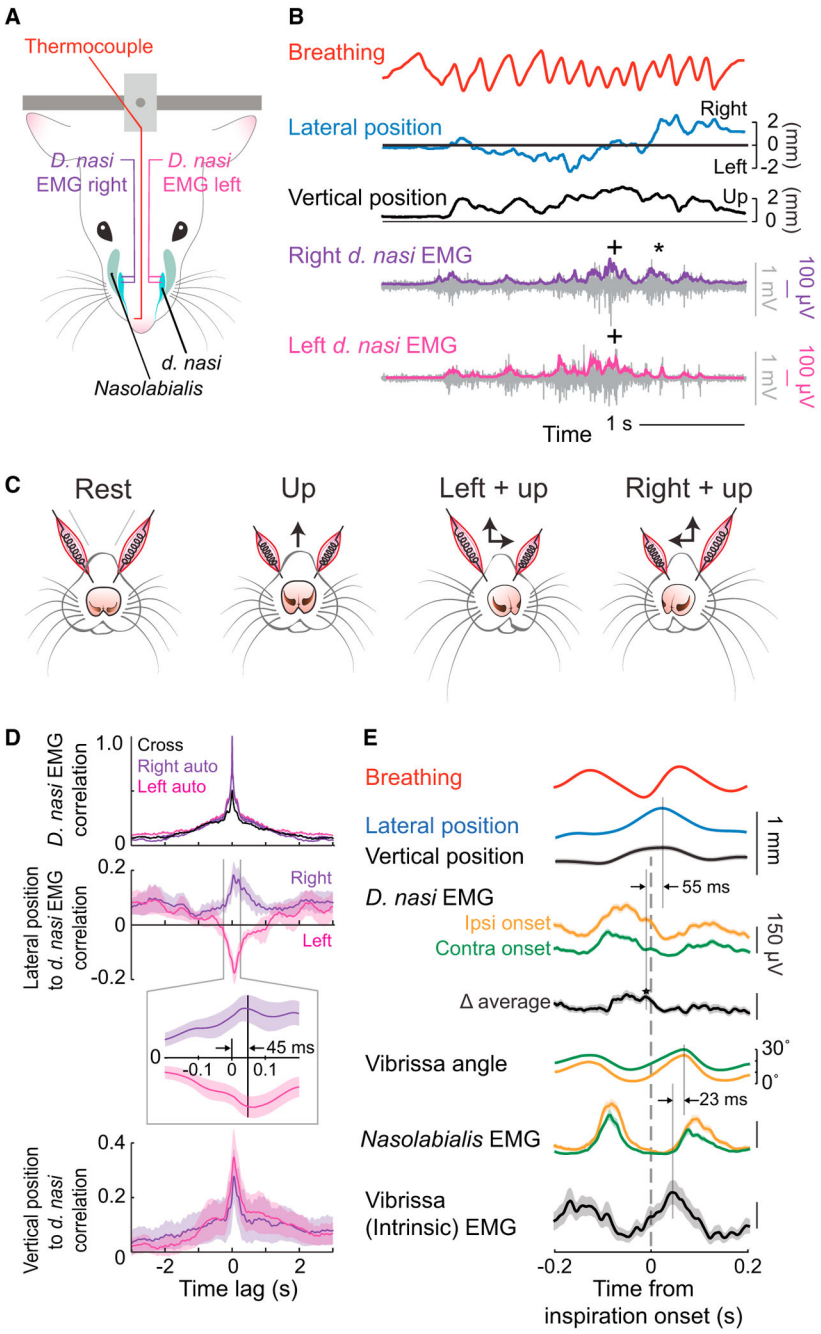


**Figure 2. Relation of EMG from Nose, Mystacial Pad, and Vibrissa Muscles to Lateral Nose Motion**

(A) Schematic of the muscles in the snout. Two arrangements of EMG signals were measured. EMG wires were placed either bilaterally in the *d. nasi*, muscles or unilaterally in the *nasolabialis*, *d. nasi*, and vibrissa intrinsic muscles. The position of the nose is recorded through a CCD camera, as in Figure 1A.

(B) Time series of lateral (blue) and vertical (black) nose position along with bilateral *d. nasi* EMG recordings. The EMG envelopes, right (purple) and left (magenta), are overlaid on the raw signal (gray).

(C) Diagram of nose movement with activation of the *d. nasi* muscles.
(D) Top traces are the normalized autocorrelation and cross-correlations of the bilateral *d. nasi* EMG envelopes. Middle traces are cross-correlations of right *d. nasi* EMG envelope with deflections of the nose to the right (purple) and left *d. nasi* EMG envelope with deflections to the left (magenta). The insert is an expansion near zero lag. Bottom traces are cross-correlations of right and left *d. nasi* EMG envelopes with vertical displacement of the nose. Data pooled across 4,000 s of data across three rats.
(E) Triggered average of lateral (blue) and vertical (black) nose position, vibrissa position, and the EMG envelope in facial muscles with respect to the onset of inspiration during 4 to 6 Hz sniffing. The EMG data from *d. nasi* were sorted by ipsilateral (orange) and contralateral (green) onset of movement prior to rectification. Data pooled from 530 epochs across six rats.

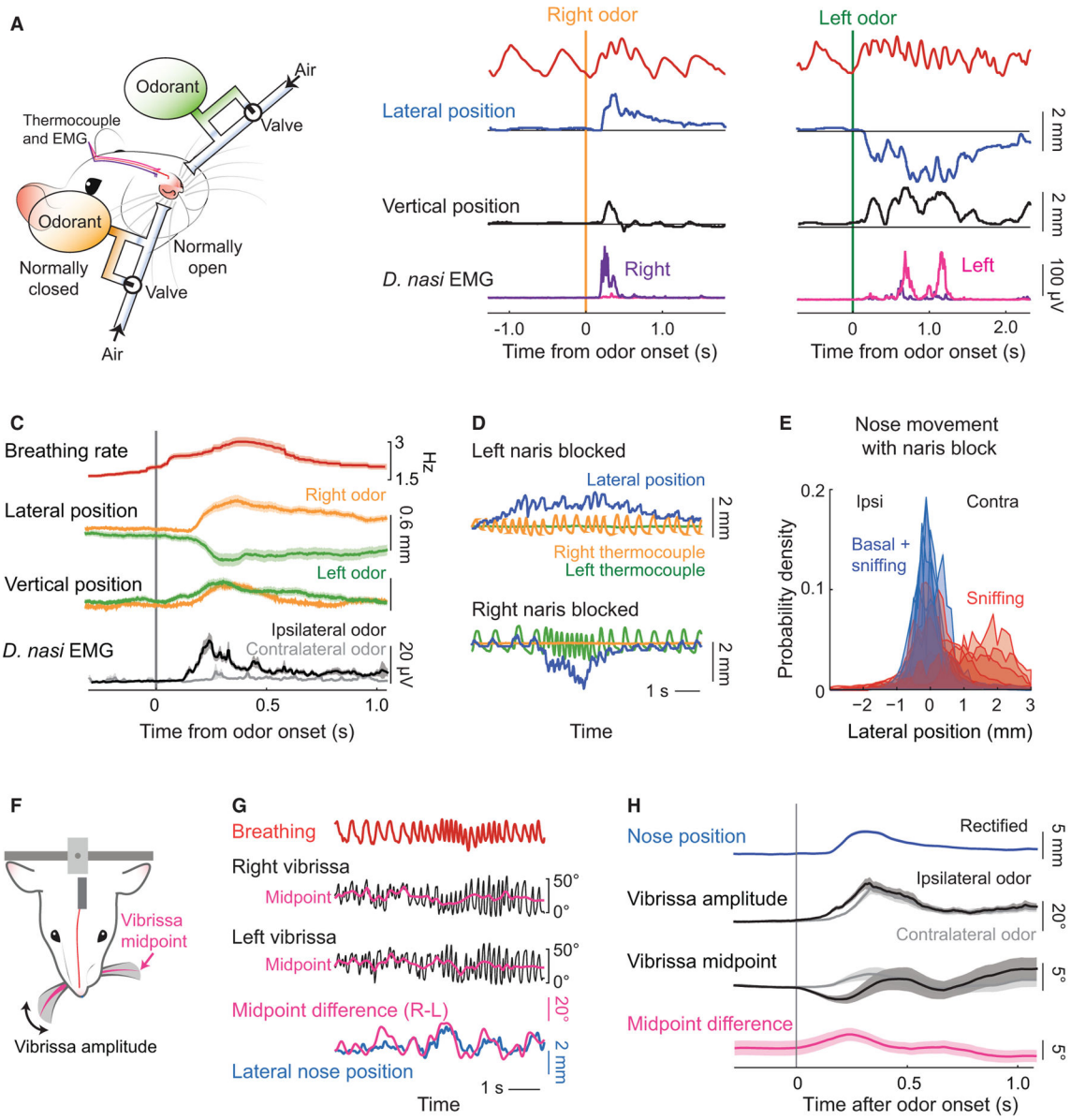


**Figure 3. Changes in the Bias of Deflection of the Nose and Vibrissae Concurrent with Odor Presentation**

(A) Schematic of the bilateral olfactometer setup. The rat is head-restrained, wired with electrodes for measuring the EMGs from the right and left *d. nasi*, and is fitted with a thermocouple to monitor breathing (Figure 2A). Bedding odor can be presented alternately on the right (orange) or left (green) side by activating one of two three-way solenoid valves that maintain constant air flow with or without an odorant.

(B) Example time series of the change in lateral (blue) and vertical (black) position, together with the right and left EMG and breathing signal, is response to bedding odor. Each of the two sets of traces is from a single trial.

(C) The average response of the envelope of the EMGs from the *d. nasi*, displayed relative to contra- versus ipsilateral presentation of odorant. We further show the average change in

lateral and vertical nose position to laterally presented bedding odor, with trials pooled by right (orange) and left (green) odor presentation. The breathing is shown as the averaged, instantaneous rate. Data pooled over 120 presentations across three rats.
(D) Example time series of lateral nose position with one naris blocked. For these measurements, the rat had two thermocouples implanted, one is each nasal cavity. The right (orange) or left (green) thermocouple signal was observed to go to zero when the corresponding naris was blocked while the other thermocouple faithfully reported breathing.
(E) Probability density function of lateral nose position distribution with one nostril blocked during all recording time (blue) and during sniffing only (red). Data pooled over 1,040 s of recordings across 6 rats.
(F) Schematic of the view of a CCD camera for tracking the vibrissae. In addition, breathing was measured with a thermocouple and the nose position was tracked in a single, front plane.
(G) Time-series of breathing (red) and the position of the left (green) and right (black) C2 vibrissa. The midpoint of whisking was computed as the average between the upper and lower envelope of the cycle-by-cycle angle of the vibrissa. The difference between vibrissa midpoints (magenta) is scaled to overlap maximally with the lateral nose position (blue).
(H) The olfactometer (A) was added to establish the response of the vibrissae to a bedding odorant. We show the time series of the whisking amplitude and midpoint along with the average nose position, rectified so that right and left deflections overlap. Trials were selected by criterion that lateral deflection of the nose in response to the odor exceeded 1 mm from rest. Data pooled from 177 trials across three rats.
See also Figure S2.

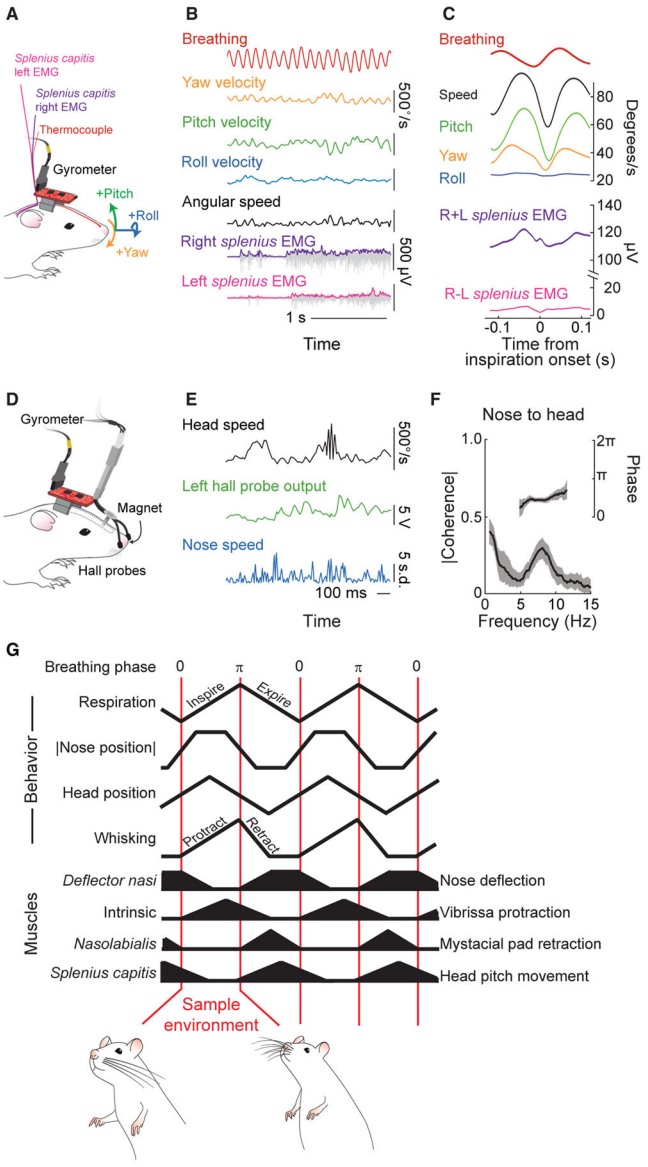


**Figure 4. Head Bobbing and Summary of Rhythmic Orofacial Motor Actions in Relation to Breathing**

(A) Schematic of the setup for measurements of head angular motion relative to the breathing cycle. A three-axis gyrometer is mounted on the head to record pitch, roll, and yaw of head movement, and a thermocouple was implanted in the nasal cavity to measure breathing. All signals were routed through a commutator.

(B) Time series of breathing (red), yaw velocity ($\omega_\alpha$; orange), pitch velocity ($\omega_\gamma$; green), and roll velocity ($\omega_\beta$; blue) of the head, along with EMG data from the right and left *splenius capitis* muscles during a sniffing bout. Angular speed (black) was computed as $\sqrt{(\omega_\alpha)^2+ (\omega_\beta)^2+(\omega_\beta)^2}$. Both raw EMG data (gray) and the envelope (magenta and purple) are shown; the scale for the envelope is 125 μV.

(C) Triggered average of breathing (red), individual angular velocities, angular speed (magenta), and the summed and difference EMG signals, with respect to the onset of

inspiration. Data pooled over three animals with 20,500 sniff cycles. The error band is a 0.95 confidence interval.

(D) Schematic of the setup for measurements of head position relative to the nose position. A three-axis gyrometer is mounted on the head to record pitch, roll, and yaw of head movement, as in (A). Nose velocity was measured by a pair of Hall-effect probes mounted around the nose and a small magnet implanted in the nasal cartilage.

(E) Time series of head speed (black), left Hall probe output (green) and normalized nose speed computed from the Hall probe signals (blue).

(F) Spectral coherence of head speed and nose speed. Data pooled from 28 epochs, lasting 830 s, over 3 animals. The error band is a 0.95 confidence interval.

(G) Summary of orofacial movements and muscle activity with respect to phase in the sniff cycle.

See also Figure S3.